7. C. Isobe and M. Saitoh, *Appl. Phys. Lett.*, **56,** 907 (1990).
8. S. Tanimoto, M. Matsui, K. Kamisako, K. Kuroiwa, and Y. Tarui, *J. Electrochem. Soc.*, **139,** 320 (1992).
9. W. S. Lau, K. K. Khaw, P. W. Qian, N. P. Sandler, and P. K. Chu, *Jpn. J. Appl. Phys.*, **35,** 2599 (1996).
10. S. C. Sun, and T. F. Chen, *IEEE Electron Device Lett.*, **EDL-17,** 355 (1996).
11. H. S. Park, Y. K. Baek, J. C. Kim, S. H. Choi, and K. H. Oh, Extended Abstracts of International Conference on Solid State Devices and Materials, Japan Society of Applied Physics, p. 524 (1992).
12. S. Kamiyama, H. Suzuki, H. Watanabe, A. Sakai, H. Kimura, and J. Mizuki, *J. Electrochem. Soc.*, **141,** 1246 (1994).
13. T. Aoyama, S. Saida, Y. Okayama, M. Fujisaki, K. Imai, and T. Arikado, *J. Electrochem. Soc.*, **143,** 977 (1996).
14. Y. Matsui, K. Torii, M. Hirayama, Y. Fujisaki, S. Iijima, and Y. Ohji, *IEEE Electron Device Lett.*, **EDL-17,** 431 (1996).
15. W. S. Lau, K. K. Khaw, P. W. Qian, N. P. Sandler, and P. K. Chu, *J. Appl. Phys.*, **79,** 8841 (1996).
16. H. Shinriki, T. Kisu, S. Kimura, Y. Nishioka, Y. Kawamoto, and K. Mukai, *IEEE Trans. Electron Devices*, **ED-37,** 1939 (1990).
17. S. Kamiyama, H. Suzuki, H. Watanabe, A. Sakai, M. Oshida, T. Tatsumi, T. Tanigawa, N. Kasai, and A. Ishitani, *Tech. Dig. Int. Electron. Devices Meet.*, p. 49 (1993).
18. T. Kaga, Y. Sudoh, H. Goto, K. Shoji, T. Kisu, H. Yamashita, R. Nagai, S. Iijima, M. Ohkura, F. Murai, T. Tanaka, Y. Goto, N. Yokoyama, M. Horiguchi, M. Isoda, T. Nishida, and E. Takeda, *Tech. Dig. Int. Electron. Devices Meet.*, p. 927 (1994).
19. A. Yuuki, M. Yamamuka, T. Makita, T. Horikawa, T. Shibano, N. Hirano, H. Maeda, N. Mikami, K. Ono, H. Ogata, and H. Abe, *Tech. Dig. Int. Electron. Devices Meet.*, p. 115 (1995).
20. P-Y. Lesaicherre, S. Yamamichi, K. Takemura, H. Yamaguchi, K. Tokashiki, Y. Miyasaka, M. Yoshida, and H. Ono, *Integ. Ferroelect.*, **11,** 81 (1995).
21. T. Aoyama, A. Murakoshi, M. Koike, S. Takeno, and K. Imai, *Jpn. J. Appl. Phys.*, **37,** L242 (1998).

Processes in Ultrathin Buried Oxide Synthesis Stimulated by Low Dose Ion Implantation

V. G. Litovchenko,* A. A. Efremov, B. N. Romanyuk, and V. P. Mel'nik

Institute of Semiconductor Physics, National Academy of Science of Ukraine, Kiev 252028, Ukraine

C. Claeys*

IMEC, B-3001 Leuven, Belgium
Katholieke Universiteit Leuven, ESAT-INSYS, B-3001 Leuven, Belgium

ABSTRACT

A low dose and moderate temperature two-stage procedure for ultrathin buried oxide preparation, using C^+ and H_2^+ implantations as stimulating factors, is proposed, theoretically studied, and experimentally validated. The process kinetics was theoretically studied by computer simulations. The optimum technological conditions are investigated and discussed in detail. Models for the induced SiO_2 synthesis are developed and compared with experimental data.

Introduction

The formation of a buried oxide layer in a Si substrate, intended for silicon-on-insulator (SOI) applications, is to a large degree controlled by complex point defect dynamics. Oxygen ions are generally implanted at elevated temperatures (~500°C) to promote dynamic annealing of the during ion implantation generated defects.[1] A very high dose (1.8×10^{18} O^+/cm^2) must be used for the formation of a stoichiometric SiO_2 buried oxide (BOX). For this reason, however, one can only form rather thick (~400 nm) BOX layers, so that the technique is not suitable for the fabrication of the thin layers needed for deep submicron technologies.[2] Postimplantation annealing at temperatures above 1300°C is needed, in order to produce device quality material.[1,2]

The high dose used in the standard process is also the main reason for the rather high cost of separation by implanted oxygen (SIMOX) material.[3] Synthesis of a relatively thin (~80 nm) and continuous buried SiO_2 layer can be achieved, however, by a low dose oxygen implantation and the same high temperature post-implantation annealing. In this case the optimal dose range is about 3.5 to 4.0×10^{17} cm^{-2}.[4] Beyond this "dose window" the continuity of the buried SiO_2 layer strongly degrades, i.e., numerous Si pipes or Si islands are left in the synthesized BOX when using a lower or high dose, respectively.[5] On the other hand, the crystalline quality of the top silicon is higher for a lower dose.[3] There are several other low dose approaches reported in the literature, such as (*i*) low energy SIMOX formation, (*ii*) two (or multi)-energy implantations, (*iii*) consecutive implantation of oxygen and nitrogen, (*iv*) varying the temperature ramping rates of the anneals, and so on.[3,6] For most of these techniques, a high temperature postimplantation annealing should be used to obtain a device-quality silicon film. Such a very high temperature anneal, however, is another reason for the high cost of a SIMOX technology.

This paper is devoted to another low-dose SOI fabrication technology, based on the use of multiple low dose oxygen ion implantation cycles. A first ion implantation with isovalent impurities, such as hydrogen or inert gas ions,[7-9] is used to create at a certain depth in the silicon, centers for oxygen precipitation and to obtain the appropriate conditions for enhanced growth of the SiO_2 phase (e.g., formation of additional free volume due to the presence of nanocavities). These additional procedures are aimed at accumulating oxygen in a very thin region and at suppressing SiO_2 precipitation outside this region. After the first and the second implantation, a standard furnace or rapid thermal annealing at relatively moderate temperatures is proposed. Also during ion implantation lower temperatures than in the standard case are used in order to make optimal use of the interaction between the different defects and impurities, to act as a driving force for enhanced nucleation. Therefore, during O^+ implantation only partial dynamic defect annealing takes place. This way of SOI preparation may be considered as a low-dose approach combined with optimized defect engineering. One of the variants of this approach, using a total oxygen implantation dose of about 2×10^{17} cm^{-2} and allowing to synthesize a 50 nm thick BOX layer, is demonstrated. This goal is achieved by optimal defect engineering, based on oxygen gettering by defects

* Electrochemical Society Active Member.

and relying on the influence of impurities (C and H) on the reaction between oxygen and silicon.[8] An optimized double implantation and annealing cycle is used here.

The main aim of the first implantation and annealing cycle is the creation of a "seed" layer. This layer is understoichiometric (30 to 45 atom % of oxygen) and mainly consists of isolated SiO_2 inclusions. During the second implantation and anneal cycle this layer effectively absorbs the additionally implanted oxygen, resulting in a continuous SiO_2 layer formation. In this paper, the main attention is given to the first stage of the process, as this is the most important one for achieving the ultrathin buried oxide formation. The physical mechanisms of the processes involved are analyzed in detail by means of computer simulations, giving information about the qualitative behavior of the system.

Physical Mechanisms and Their Modeling

The physical oxidation mechanisms, taking place in the low-dose SIMOX approaches, seem to be more complicated than those occurring in the conventional case. The most important processes during buried oxide (BOX) synthesis which are considered are (*i*) the quasi-chemical reactions between implanted species and defects, (*ii*) their diffusion and pairing, (*iii*) the initial stage of SiO_2 precipitate growth/decomposition, (*iv*) their coalescence, and (*v*) the final stage of the layer-by-layer growth of the stoichiometric buried oxide.

Hence, to analyze the process going on during enhanced BOX formation one should take into account multiple quasi-chemical reactions between oxygen and different defects and complexes present in the silicon. In order to study these processes we have written several versions of code SYNTHESIS, which considers the problem of ion beam induced new phase formation from different points of view. The first one[9] treats the buried layer growth as a growth and decomposition of SiO_2 precipitates (different in size) up to the stage where they merge with each other into a continuous layer. In this paper, another physical approach, based on a quasi-chemical description of the processes involved, is used. The code calculates the solution of a set of differential equations describing the diffusion, drift, and reactions for all components of the system which behavior is important for the process studied.

The code is based on the mathematical technique of finite differences and easily allows changing the number of equations involved and the values of their coefficients

$$\partial C_k/\partial t = D_k \partial^2 C_k/\partial z^2 + R_k(C_1, C_2, ..., C_n) + g_k(z) \quad [1]$$

Here C_k is the volume concentration of the kth component of a system (foreign or matrix atoms or defects) which can diffuse with diffusivity, D_k, and interact with other components according to a nonlinear function $R_k(C_1, C_2, ..., C_n)$. Besides, incoming of the kth component due to either implantation of corresponding atoms or generation of primary defects is described by a distributed power source function $g_k(z)$. The respective functions are available either from Burenkov's tables[10] or from transport of ions in matter (TRIM) calculations.

Experimental

Czochralski (CZ) (100) oriented silicon wafers with a resistivity of 10 Ω cm were implanted with O^+ ($D_o = 1 \times 10^{17}$ cm^{-2} and $E = 150$ keV). After this a C^+ implantation ($E = 50$ to 150 keV) was carried out with different doses. Subsequently, the samples were annealed at $T_A = 1150$°C in an Ar ambient. After annealing a second O^+ implantation with $D_o^* = 1 \times 10^{17}$ cm^{-2} and an additional annealing at $T_A^* = 1250$°C were performed. The influence of an initial H_2^+ implantation at $D_{H_2} = (2\text{-}10) \times 10^{16}$ cm^{-2} and $E = 60$ keV, instead of a C^+ implantation, on the buried oxide formation was studied under the same conditions for the O^+ implantations. The depth distribution of the implanted species was studied by Auger electron spectroscopy (AES). The depth distribution of the mechanical stress was obtained for O^+ and (O^+ and C^+) implanted and annealed samples from Raman spectroscopy data, using sequential ion sputtering of the sample.

Carbon Induced Effects

Experimental results.—In general, the experimental AES depth profiles of oxygen in the (O^+ + C^+) implanted samples after the first annealing show three maxima.[11] The first one is located at the depth corresponding with the projected range of the carbon implantation $R_p(C^+)$. The second one is slightly shifted toward the silicon surface and is related to the projected range of the oxygen implantation $R_p(O^+)$. When $R_p(C^+)$ is equal to about 0.9 $R_p(O^+)$, these two maxima are merged into one peak. This is illustrated in Fig. 1, showing the AES oxygen depth profile after the first (O^+ + C^+) implantation, after a subsequent anneal, and after the second O^+ implantation and anneal. After the first implantation, a rather broad oxygen profile is observed (Fig. 1, curve 1). The first anneal step leads to a more defined oxygen profile (±40% height and 25 nm half-width), and also introduces in the seed layer a small additional peak with about 5% oxygen, located at a depth of 0.6 $R_p(O^+)$ (Fig. 1, curve 2). This new peak further grows (up to about 12%) during the second oxygen implantation and anneal cycle (Fig. 1, curve 3). The oxygen accumulation efficiency during the first cycle of the process depends nonmonotonously on the energy of the C^+ implantation, as illustrated in Fig. 2. As can be seen, also the half-width of the oxygen profile is influenced by the energy of the C^+ implantation. The highest oxygen accumulation is observed for the optimum case, i.e., for $R_p(C^+) = 0.9\ R_p(O^+)$.

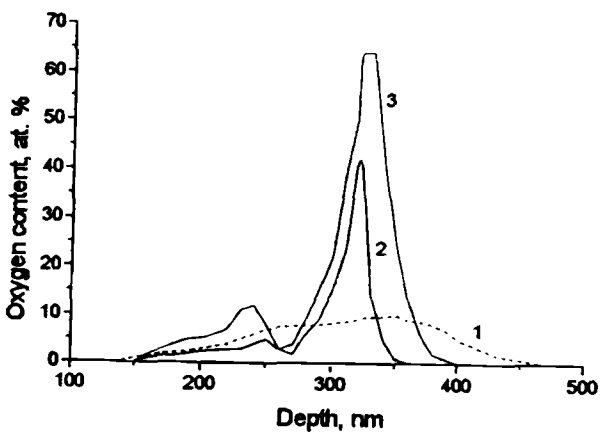

Fig. 1. Oxygen AES profile for (1) as-implanted samples after the first combined (O^+ + C^+) implantation, (2) after a subsequent anneal, and (3) after the second implantation and anneal cycle. $R_p(C^+)$ is about 0.9 $R_p(O^+)$.

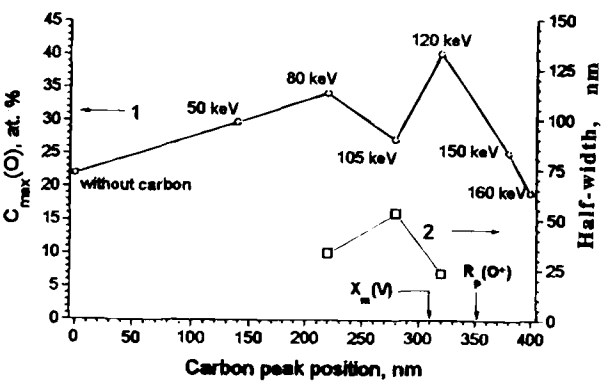

Fig. 2. Dependence of the maximum oxygen concentration (1) and the half-width of the peak (2) on the depth position of the maximum of the implanted carbon, after the first implantation and anneal cycle.

It has been shown previously[8] that this effect also depends on the C^+ implant dose and on the anneal temperature.

The process of the seed layer formation proves to be very sensitive to both the dose D_o and the temperature T_{imp} of the oxygen implantation. If D_o and T_{imp} were higher than some critical values, intensive growth of isolated precipitates in a rather wide depth range has been observed. The second stage oxygen implantation and annealing at 1250°C results in the formation of an ultrathin stoichiometric (~67% of oxygen) SiO_2 buried layer. The layer thickness d is about 15 nm (Fig. 1, curve 3). It should be noted that the temperatures used here are much lower than the commonly used ones (~1320°C). In the close vicinity of this stoichiometric layer, i.e., about 50 nm from its interfaces, small SiO_2 precipitates are formed both in the bulk and in the top silicon film. In the case of an O^+ implantation, only (without carbon implantation), the top Si layer is characterized by high values of tensile stress ($\sim 2 \times 10^8$ Pa). On the contrary, for combined ($O^+ + C^+$) implanted structures a nearly complete stress compensation ($<3 \times 10^7$ Pa) takes place.

Modeling and discussion.—As mentioned previously, in the case that only oxygen has been implanted, a high compressive stress was developed in the samples during the growth of SiO_2 inclusions in the seed layer. The main reason for using an initial carbon implantation is based on its tendency to form additional free volume to accommodate SiO_2 nuclei and precipitates due to the low value of its covalent radius. Indeed, Si–C particles in silicon produce a volume contraction of about 50%.[12] Moreover, this free volume leads to a decrease of the critical radius, r_c, of the SiO_2 nuclei.[12,13] Depending on the critical radius, the oxygen precipitates will either further grow or dissolve during the temperature treatment. On the other hand, C–O complexes are also assumed to be involved in the precipitation process itself, as they most probable act as nuclei.[13] Another stimulating factor active in our case is the vacancy clusters formed as a result of the evolution of the primary ion beam induced vacancies.[13,14] These clusters, as well as Si–C, play an important role in relieving the volume misfit associated with precipitate growth.[12-14] It is assumed that the small additional peak described above (Fig. 1, curves 2 and 3) is caused by that part of the oxidation process, which is stimulated by vacancies and vacancy complexes generated during the diffusion and redistribution of these defects between the external silicon surface and the main oxidation reaction zone.

The third important agent involved in the processes considered here are silicon interstitials. They are generated both during ion stopping and during growth of the SiO_2 inclusions. Another permanent source and sink of self-interstitials in our case may be the silicon wafer surfaces.[15] According to Abe et al.,[16] self-interstitials are introduced into the bulk after a rapid temperature rise, which always takes place during high temperature annealing. The important role of this transient stage of the annealing in BOX synthesis was original reported by Cerofolini et al.[3] and later on used in practice by Ogura.[6] Self-interstitials are responsible for a retardation and suppression of the precipitation process,[12-14] and for the dissolution of already present SiO_2 precipitates. A theoretical study of SiO_2 nucleation clearly points out the increase of the critical radius, r_c, of the precipitates in the presence of interstitials[13]

$$r_c = 2\sigma/(DG_{ch} - DG_{el}) \quad [2]$$

where σ is the interface energy per unit area, $DG_{ch} = [(1 - \epsilon)^{-3} xkT/W_p) \ln(C_{OX}/C^*_{OX})(C_V/C^*_V)^{\beta}(C_I/C^*_I)^{\gamma}$ is the general relation for the chemical energy of supersaturation per unit volume, C_{OX}, C_V, and C_I are the concentration of oxygen, vacancies, and self-interstitials in the silicon matrix, and C^*_{OX}, C^*_V, and C^*_I are the respective equilibrium concentrations. The second term in the denominator $DG_{el} = 6\mu\delta\epsilon$ is the change in the total elastic energy of a spherical nucleus related to the unit volume variation. Here μ is shear modulus of silicon, $\delta = [(W_p/W_m) - x(\beta + \gamma)]^{1/3} - 1$ is the linear misfit, and ϵ is the constrained strain. W_p and W_m are the volumes per silicon atom in the precipitate and in the matrix, respectively, x is the oxygen/silicon ratio in the SiO_x precipitate, γ and β are the numbers of self-interstitials and vacancies emitted and absorbed (per oxygen atom) by a precipitate, respectively, and further involved in the partial strain relief. Finally, the presence of self-interstitials results in a dissolution of vacancy complexes.[12] This complex interaction between different factors acting in opposite directions creates necessary conditions for spatially nonuniform SiO_2 growth, self-supported in some local regions and suppressed in other ones.

Taking into account the above mentioned interactions, one can derive the following set of quasi-chemical reactions. "Ordinary" oxidation of silicon accompanied by Si interstitials injection

$$(1 + y)\mathrm{Si} + 2\,\mathrm{O} \rightarrow \mathrm{SiO_2} + y\mathrm{I} \quad [3]$$

Two-step oxidation of silicon, whereby the intermediate phase is being stabilized with vacancies or/and vacancy complexes

$$\mathrm{Si} + \mathrm{O} + (n)V \rightarrow \mathrm{SiO} \quad [4]$$

$$\mathrm{SiO} + (n)V + \mathrm{O} \rightarrow \mathrm{SiO_2} \quad [5]$$

Reactions 3 and 4 take into account the silicon oxidation promoted by vacancies.

The metastable SiO phase has to decompose into SiO_2 and Si, mainly due to the mechanical stress. This process consists in a local spatial redistribution of oxygen atoms and does not require an additional one as in reaction 4. It is assumed, however, that it proceeds more efficiently in the presence of SiO_2 nuclei, acting as centers of phase separation. Therefore, this process can be described by the quasi-chemical reaction

$$\mathrm{SiO_2} + 2\mathrm{SiO} \rightarrow 2\mathrm{SiO_2} + \mathrm{Si} \quad [6]$$

It is observed that the stress compensation takes place only under optimum conditions and for a relatively low carbon dose, equal to about 5% of the oxygen dose.[8] Calculations point out, however, that this concentration is surely not enough to obtain a complete compensation. Therefore, here the carbon atoms should act via some indirect self-supporting mechanism. Two possible models are further proposed to explain this.

In the first model, it is supposed that carbon (together with vacancies) acts only at the initial stage of the SiO_2 nuclei growth, providing an enhanced oxidation in some narrow local regions by means of reactions such as

$$\mathrm{Si} + V + \mathrm{C} \rightarrow \mathrm{SiC} \quad [7]$$

$$\mathrm{SiC} + \mathrm{O} \rightarrow \mathrm{SiCO} \quad [8]$$

$$\mathrm{SiCO} + \mathrm{O} \rightarrow \mathrm{SiO_2} + \mathrm{C} \quad [9]$$

Hence, temporary C–O pairs or/and SiC bonds are formed and an excess of free volume for the Si–O–Si bridge accommodation becomes available. As a result, a total stress compensation is achieved during the initial stages of nucleation and growth. Besides, the carbon atoms released in reaction 9 are not incorporated into the silicon matrix, but into the SiO_2 phase. So, the carbon atoms lead only to an initial enhancement of the growth, sufficient for the formation of large enough (i.e., supercritical $r > r_c$) SiO_2 nuclei in a narrow region of the sample. Subsequent growth of these precipitates occurs via reaction 3 and is accompanied by an injection of self-interstitials. These self-interstitials suppress the growth of other neighboring small SiO_2 inclusions and result in their decomposition due to the reverse reaction 3.[12] The complete stress compensation probably takes place due to a change of the shape of the precipitates from spherical to disk-like during their growth.[7] It can be noticed that for the realization of this mechanism, only a low carbon concentration is necessary and sufficient.

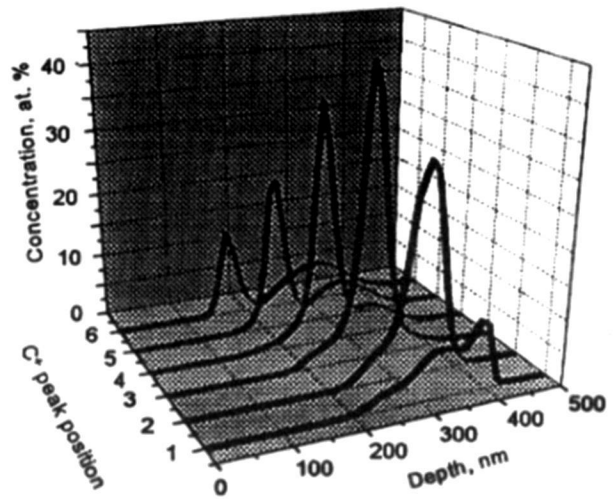

Fig. 3. Spatial distribution of the bounded oxygen ($R_p(O^+)$ = 350 nm) vs. implanted carbon peak at position (1) $R_p(C^+)$ = 400 nm, (2) $R_p(C^+)$ = 350 nm, (3) $R_p(C^+)$ = 300 nm, (4) $R_p(C^+)$ = 250 nm, (5) $R_p(C^+)$ = 200 nm, and (6) $R_p(C^+)$ = 150 nm.

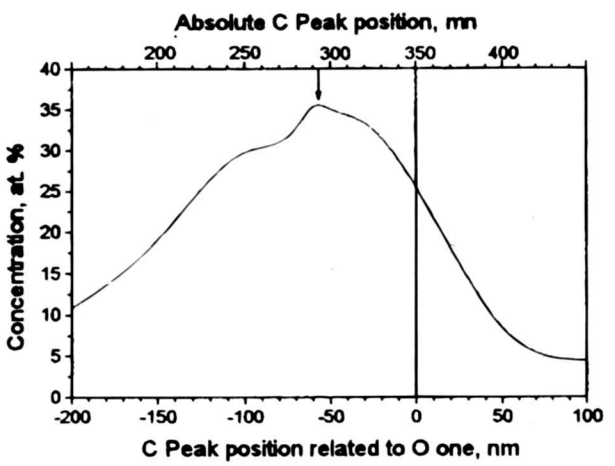

Fig. 4. Calculated oxygen concentration in the maximum of the distribution vs. the position of the implanted C^+ peak.

In the second model, the same set of reactions is assumed, but in contrast to the previous case the carbon atoms released in reaction 9 are assumed to be pushed out of the SiO_2 into the adjacent silicon lattice. So, a recurrent carbon utilization is possible here and reactions 7 to 9 can repeat again. In this model also only a small concentration of carbon, playing a catalytic role, is necessary. The results of calculations in the framework of this last model are presented in Fig. 3 and 4. The diffusion of oxygen and vacancies in the Si matrix is taken into account according to Eq. 1.

Figure 3 shows the dependence of the shape of the spatial distribution of the oxygen concentration in the seed layer on the position of the carbon implantation peak $R_p(C^+)$. One can see that if the carbon implantation peak is located either far in front or far behind the oxygen implantation maximum $R_p(O^+)$, the oxygen distribution splits into two wide peaks. If carbon is implanted into a region near the maximum of the oxygen distribution, the two peaks coincide and a sharp narrowing of the peak takes place. A rather poorly defined maximum, attributed to pure "vacancy-induced" oxidation, is also observed (curves 1, 2, 3) in front of the main peak. The most substantial narrowing and oxygen accumulation is observed at $R_p(C^+) = (0.8 - 0.9)\ R_p(O^+)$, in a good agreement with experimental observations. The maximum value of the oxygen concentration as a function of the relative position of $R_p(C^+)$ and $R_p(O^+)$ is shown in Fig. 4. The optimum peak position of the carbon obtained from the calculations is practically the same as the experimentally observed one. The model also predicts roughly a "drop" of the maximum value of the concentration at $R_p(C^+)$ 270 nm (see Fig. 2 and 5).

Both calculations and experiments point out that there are three different mechanisms acting in the same direction: ordinary formation of SiO_2 inclusions due to oversaturation (rate constant K_O), SiO_2 growth stimulated by vacancies (rate constant K_V), and stimulated growth caused by the presence of carbon (rate constant K_C). There are four characteristic regions in the curves given the experimental (Fig. 2) and theoretical dependences (Fig. 3).

1. $R_p(C^+) < 0.35\ R_p(O^+)$. Here the degree of oxygen accumulation increases monotonously with $R_p(C^+)$. So the role of carbon atoms increases with an increase of the vacancy concentration. It depends also on the diffusion transport of implanted oxygen from the maximum of the distribution towards the carbon enriched region. As is clear from Fig. 3, in this case some competition between carbon-induced and vacancy-induced (or "ordinary" oxidation) processes takes place (Fig. 3, curve 6).

2. At $R_p(C^+) = 0.6\ R_p(O^+)$, one has a local minimum and there are two maxima in the oxygen depth distribution, since there exist two separated regions of preference for SiO_2 nucleation and growth in this case. (Fig. 3, curve 5.)

3. These two regions coincide when $R_p(C^+) = (0.8 - 0.9)\ R_p(O^+)$ and some cumulative effect takes place. At this point the highest value of the oxygen concentration is achieved when both mechanisms act in the same direction at the same place.

4. When $R_p(C^+) > 1.2\ R_p(O^+)$, the important agent related to the primary beam generated vacancies and vacancy complexes practically does not take part in the process (curve 1) at the location where carbon was implanted. It is accompanied by an extension of the bounded oxygen distribution and predominates the formation of different carbide phases. The latter was shown by both computer simulation and experimental depth profiling. The calculations allow one to conclude that during the first stage the reaction rate constants for stimulated confined oxidation under moderate annealing temperatures proves to be at least three orders of magnitude higher than for ordinary oxidation: $K_O:K_V:K_C$ = 1:1000:2000. The values of the reaction constants used in calculations are summarized in Table 1.

Hydrogen Induced Effects

Experimental results.—In the case of H_2^+ instead of C^+ implantation into O^+ implanted structures, some particular features can be observed. As shown in Fig. 5 and 6, an H_2^+ implantation at a depth of about 320 nm leads to a very

Table I. Rate constants for the various reactions in the carbon induced process.

No.	Reaction type	Comments	Rate constant
1.	$2Si + 2O \rightarrow SiO_2 + I$	Ordinary oxidation	$K_{do} = 1 \times 10^{-4}$ nm^{-6}/s
2.	$Si + V + O \rightarrow SiO$	Suboxide phase formation	$S_{sio} = 1 \times 10^{-4}$ nm^{-6}/s
3.	$SiO + V + O \rightarrow SiO_2$	SiO_2 phase formation enhanced by defects	$S_{dox} = 0.1$ nm^{-6}/s
4.	$SiO_2 + 2SiO \rightarrow 2SiO_2 + Si$	SiO phase decomposition induced by the SiO_2 phase	$S_{Phs} = 0.1$ nm^{-6}/s
5.	$Si + V + C \rightarrow SiC$	Intermediate carbide phase formation	$C_{siC} = 0.1$ nm^{-6}/s
6.	$SiC + O \rightarrow SiCO$	Carbon-oxygen pairing	$C_{SOC} = 0.1$ nm^{-3}/s
7.	$SiCO + O \rightarrow SiO_2 + C$	Carbon-induced oxidation	$C_{dox} = 0.2$ nm^{-3}/s

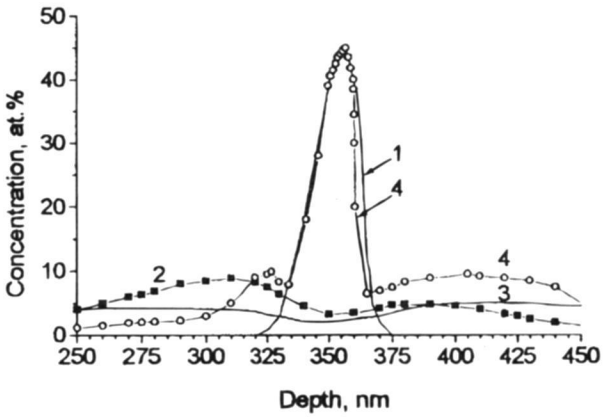

Fig. 5. Comparison between the theoretical (1, 2, and 3) and the AES depth profile (4) for O^+ and H^+ implantation and anneal. (1) ultra thin unstressed SiO_2^* phase, (2) ordinary (stressed) SiO_2 precipitates, and (3) bounded oxygen interstitials.

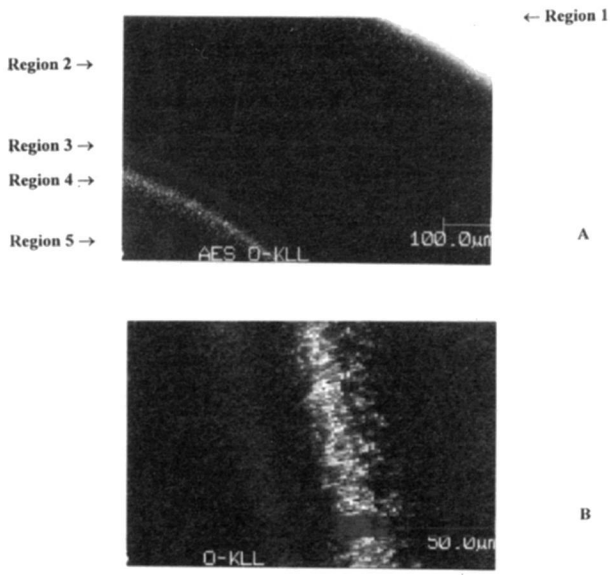

Fig. 6. AES microscopy data (O-KLL signal of oxygen) for the subsurface region of the silicon, after a combined (O^+ + H^+) implantation. (1) is the surface SiO_2 film, (2) is the top silicon film, (3) is a satellite layer, consisting of small SiO_2 inclusions, (4) is the main seed for the SiO_2 layer, and (5) is the silicon substrate. A and B correspond to different magnifications.

narrow seed layer for buried oxide formation with a thickness d = 15 to 25 nm. However, at $D_{H_2} > 5 \times 10^{16}$ cm^{-2} blistering and surface erosion are observed. The diameter and the surface density of the bubbles depend on the implantation dose. Some preliminary experiments have been performed in order to avoid the occurrence this effect.

Modeling and discussion.—A lot of information about hydrogen in silicon, and the interaction between H and different types of defects and impurities is available in the literature.[17] The model proposed here is based on the model of Cerofolini et al.,[17] but has been modified in order to take into account the formation of nanocavities and their possible influence upon oxygen precipitation.

The proposed model is built up by using the following set of considerations:

1. The following hydrogen-related reactions are taken into account

ordinary association	$H + H \rightarrow H_2$	[10]
trapping by the defects	$X + H \rightarrow XH$ (Si–H)	[11]
autocatalytic association	$XH + H \rightarrow X + H_2$	[12]

Here X is some unspecified (vacancy containing) structural defect, e.g., a divacancy, etc., formed after ion implantation. The results described in Ref. 18 allow the assumption that the depth distribution of such defects is proportional to the depth distribution of Frenkel defects, as also observed in the nuclear energy transfer distribution obtained by TRIM simulations.

2. Subsequently, the formation of nanoblisters is treated in a somewhat simplifying form. The formation of elementary nanobubble (ENB) with simultaneous self-interstitial injection into the matrix proceeds according to the reaction

$$H_2 + H_2 \rightarrow ENB + 2I \quad [13]$$

Each ENB contains only two H_2 molecules. It is supposed, that a real nanoblister may be treated as clusters of ENBs. The introduction of ENBs allows one to apply the quasi-chemical approach to the problem of bubble formation under oxidation without, however, a detailed description of the nanobubble growth as this is out of the scope of the present paper.

3. The interaction of oxygen with silicon is considered in two aspects: "ordinary" oxidation, accompanied by stressed SiO_2 precipitates growth and Si interstitial injection (reaction 3) and an enhanced oxidation of silicon in the local vicinity of the nanobubbles. In the latter case unstressed growth of precipitates takes place without any initial (stress or interstitials induced) barrier

$$ENB + Si + 2O \rightarrow SiO_2^* \quad [14]$$

In order to clearly distinguish this unstressed SiO_2 phase, which is formed in silicon enriched with nanocavities due to reaction 14, from the ordinary stressed SiO_2 precipitates formed due to reaction 3 the former is indicated as SiO_2^* (i.e., with star). Reaction 14 results in a disappearance of one elementary nanobubble due to the consumption of available free volume. These unstressed SiO_2^* inclusions which are formed may grow further in the usual way

$$SiO_2^* + Si + 2O \rightarrow 2SiO_2^* \quad [15]$$

4. The generation and redistribution of Si interstitials during annealing, including some temperature enhancement effects,[3,6] are taken into account. In our case, at least two processes, SiO_2 precipitation and ENB formation, are accompanied by an injection of additional self-interstitials. It is also supposed that during the temperature ramping self-interstitials are emitted from the surface.[15,16] Therefore, the above set of reactions can be extended in order to include in the model a reaction for the stimulated decomposition of stressed SiO_2 inclusions

$$SiO_2 + yI \rightarrow (1 + y)Si + 2O \quad [16]$$

In addition, all induced defects which involve vacancies and which were above referred to as X, can also absorb interstitials

$$X + I \rightarrow Si \quad [17]$$

The values for the reaction parameters used in calculations are summarized in Table II.

The computer simulation of the annealing after the combined H_2^+ and O^+ implantation takes into account reactions 10 to 17, and the diffusion of Si interstitials, vacancies (or X-defects), O, H, and H_2. The results are presented in Fig. 5. One can observe a rather good agreement between the simulated (curve 1) and the experimental oxygen profiles (curve 4), both in width and shape. Simulation shows, however, that the final result of the synthesis is very sensitive to the intensities of the different types of reactions treated in the model. Therefore, a very narrow buried seed layer may be formed only under optimum conditions of both implantation and annealing. This will be achieved also under optimum rates of second-order reactions such as Eq. 13 and 16.

The most important feature of the initial stage of hydrogen-enhanced synthesis is a rapid growth of ordinary

Table II. Rate constants for the various reactions in the hydrogen induced process.

NN	Reaction type	Comments	Rate constant
1.	$Si + 2\,O \rightarrow SiO_2 + 2I$	Ordinary oxidation: stressed SiO_2 inclusions	$K_{dox} = 10^{-4}$ nm^{-6}/s
2.	$Si + 2\,O + ENB \rightarrow SiO_2^*$	Enhanced oxidation: unstressed dioxide phase SiO_2^* nucleation	$B_{dox} = 10^{-2}$ nm^{-9}/s
3.	$SiO_2^* + Si + 2\,O \rightarrow 2SiO_2^*$	Growth of unstressed SiO_2^* phase	$G_{nb} = 10^{-4}$ nm^{-9}/s
4.	$SiO_2 + 2I \rightarrow 3Si + 2O$	SiO_2 decomposition induced by interstitials	$D_{ec} = 10^{-2}$ nm^{-6}/s
5.	$X + I \rightarrow Si$	Frenkel's pair recombination	$R_{iv} = 0.05$ nm^{-3}/s
6.	$H + H \rightarrow H_2$	Ordinary association	$R_{HH} = 10^{-2}$ nm^{-3}/s
7.	$H + X \rightarrow XH$	Hydrogen trapping by ion induced defects	$K_{VH} = 10^{-2}$ nm^{-3}/s
8.	$XH + H \rightarrow X + H_2$	Autocatalytic hydrogen association	$A_{HH} = 10^{-2}$ nm^{-3}/s
9.	$H_2 + H_2 \rightarrow ENB + 2I$	Elementary nanobubble formation	$K_{NB} = 10^{-2}$ nm^{-3}/s

(stressed) SiO_2 inclusions accompanied by self-interstitials generation with the subsequent formation of the SiO_2^* phase in a narrow layer near the R_p for hydrogen. The optimum condition for this case is a coinciding of the R_p for oxygen and hydrogen. Indeed, according to Eq. 2 for strain-free SiO_2 nucleation (which takes place in the silicon region containing nanocavities), the critical precipitate radius, r_c, has its minimum value at the depth where the oxygen concentration has its maximum, i.e., at $R_p(O^+)$. The oxygen content within this narrow layer continues to increase without increasing its thickness if the rate of ENB formation (Eq. 13) is low enough in comparison to the rate of enhanced oxidation in the vicinity of the nanobubbles (Eq. 14). Therefore, the production of large nanoblisters by a higher dose H_2^+ implantation is undesirable in our case.

Conclusion

Two different variants of a low-dose approach with optimized defect engineering technique for SOI preparation have been theoretically studied and experimentally demonstrated. The approach includes a two-stage low dose oxygen implantation and annealing. The aim of the first implantation and anneal cycle is the creation of an understoichiometric seed layer (30 to 45 atom % of oxygen). After the first stage the centers for enhanced precipitation and rapid initial growth are introduced in a well-defined location relative to the oxygen peak. Such centers may be created by ion implantation of either carbon or hydrogen at definite doses. These additional procedures are aimed at an accumulation of oxygen in a very thin region and at a suppresion SiO_2 precipitation in the silicon outside this region.

In the case of carbon, the stimulating factors are (*i*) creation of additional local free volume to accommodate the SiO_2 precipitates, (*ii*) generation of additional vacancies and vacancy complexes, and (*iii*) the fact that stress compensation seems to be involved in the process. In the case of hydrogen the main factor resulting in a super thin SiO_x seed layer formation is the strain-free selective oxidation of silicon in a close vicinity of the created nanobubbles. However, complex interactions between different types of defects and precipitates are found to be also important in this process.

During the second cycle of oxygen implantation and annealing the seed layer effectively absorbs the additionally implanted oxygen, resulting in a continuous SiO_2 layer formation. For the considered approach a moderate temperature of implantation and annealing and a low total dose of oxygen implantation ($D_O = 2 \times 10^{17}$ cm^{-2}) have to be used. This allows for an increase in both the relative role of defect supersaturation instead of oxygen supersaturation as a driving force for nucleation (Eq. 2), and the role of stress controlled precipitation. The thickness of the buried layer (~50 nm) obtained in such a manner is thinner than has been reported before.

The codes developed for the computer modeling of the ion-beam synthesis of buried layers has proven to be very suitable and reliable, both for studying the physical processes and for optimizing the technological manufacturing parameters.

Acknowledgments

This work was partly supported by STCU grant no. 382.

Manuscript received December 29, 1997.

REFERENCES

1. S. T. Pantelides and M. Ramamoorthy, in *Silicon on Insulator Technology and Devices*, S. Cristoloveanu, P. L. F. Hemment, K. Izumi, and S. Wilson, Editors, PV 97-23, p. 39, The Electrochemical Society Proceedings Series, Pennington, NJ (1997).
2. J. A. Auberton-Herve, B. Aspar, and J. L. Pelloie, in *Physical and Technical Problems of SOI Structures and Devices*, J. P. Colinge, Editor, p. 3, Kluwer Academic Publishers, Dortrecht (1994).
3. G. F. Cerofolini, S. Bertoni, L. Meda, and C. Spaggiari, *Semicond. Sci. Technol.*, **11**, 398 (1996).
4. S. Nakashima and K. Izumi, *J. Mater. Res.*, **8**, 523 (1993).
5. J. Jablonski, M. Saito, Y. Miyamura, and T. Katayama, in *Silicon on Insulator Technology and Devices*, S. Cristoloveanu, P. L. F. Hemment, K. Izumi, and S. Wilson, Editors, PV 97-23, p. 51, The Electrochemical Society Proceedings Series, Pennington, NJ (1997).
6. A. Ogura, in *Silicon on Insulator Technology and Devices*, S. Cristoloveanu, P. L. F. Hemment, K. Izumi, and S. Wilson, Editors, PV 97-23, p. 57, The Electrochemical Society Proceedings Series, Pennington, NJ (1997).
7. V. Litovchenko, B. Romanyuk, A. Efremov, and V. Melnik, in *Physical and Technical Problems of SOI Structures and Devices*, J. P. Colinge, Editor, p. 73, Kluwer Academic Publishers, Dortrecht (1994).
8. V. Litovchenko, B. Romanyuk, A. Efremov, and V. Melnik, in *Silicon on Insulator Technology and Devices*, P. L. F. Hemment, S. Cristoloveanu, K. Izumi, T. Houston, and S. Wilson, Editors, PV 96-3, p. 117, The Electrochemical Society Proceedings Series, Pennington, NJ (1996).
9. V. Litovchenko, B. Romanyuk, and A. Efremov, in *Formation of Semiconductor Interfaces, IFES-4*, B. Lengeler, Editor, p. 389, World Science Publishers, London (1993).
10. A. F. Burenkov, F. F. Komarov, M. A. Kumachov, and M. M. Temkin, *Spatial Distribution of Energy Deposited within a Cascade of Atomic Collisions in Solids*, Energoatomizdat, Moscow (1985) (in Russian).
11. B. Romanyuk, N. Klui, D. Kruger, et al., in *Optoelectronics and Semiconductor Technics*, **31**, Naukova Dumka, Kiev, p. 159 (1996) (In Ukrainian).
12. A. Borghesi, B. Pivac, A. Sasela, and A. Stella, *J. Appl. Phys.*, **77**, 4169 (1995).
13. J. Vanhellemont and C. Claeys, *J. Appl. Phys.*, **62**, 3960 (1987).
14. J. Vanhellemont and C. Claeys, *J. Electrochem. Soc.*, **135**, 1509 (1988).
15. Y. Satoh, H. Furuya, Kadoi, and Y. Shimanuki, *J. Appl. Phys.*, **77**, 3710 (1995).
16. H. Abe, I. Suzuki, and H. Koya , *J. Electrochem. Soc.*, **144**, 306 (1997).
17. G. Cerofolini, R. Balboni et al., *Phys. Status Solidi*, **150**, 539 (1995).
18. D. Fink, J. Krauser, D. Nagengast et al., *J. Appl. Phys. A*, **61**, 381 (1995).